Toughened Nylon66/Nylon6 Ternary Nanocomposites by Elastomers

Jun Chen, Wei Wu, Chuan Chen, Sanxiong He

Sino-German Joint Research Center of Advanced Materials, School of Materials Science and Technology, East China University of Science and Technology, Shanghai 200237, People's Republic of China

Received 16 November 2008; accepted 22 June 2009
DOI 10.1002/app.30989
Published online 8 September 2009 in Wiley InterScience (www.interscience.wiley.com).

ABSTRACT: The elastomer toughening of PA66/PA6 nanocomposites prepared from the organic modified montmorillonite (OMMT) was examined as a means of balancing stiffness/strength versus toughness/ductility. Several different formulations varying in OMMT content were made by mixing of PA6 and OMMT as a masterbatch and then blending it with PA66 and different elastomers in a twin screw extruder. In this sequence, the OMMT layers were well exfoliated in the nylon alloy matrix. The introduction of silicate layers with PA6 induced the appearance of the γ crystal phase in the nanocomposites, which is unstable and seldom appears in PA66 at room temperature and it further affected the morphology and dispersion of rubber phase resulting in much smaller rubber particles. The incorporation of POE-*g*-MA particles toughened the nanocomposites markedly, but the tensile modulus and strength were both reduced. Conversely, the use of OMMT increased the modulus but decreased the fracture toughness. The nanocomposites exhibited balanced stiffness and toughness. © 2009 Wiley Periodicals, Inc. J Appl Polym Sci 115: 588–598, 2010

Key words: nylon 66; nylon 6; elastomer; montmorillonite; nanocomposite

INTRODUCTION

Polyamides 6 (PA6) and polyamide 66 (PA66) are widely used materials because of their tunable properties and account for the majority of commercial polyamide production and application. They hae been extensively applied in the fields of vehicles, electronic appliances, and sophisticated machinery, owing to its good mechanical strength and chemical resistance.

Polyamide 6 (PA6) and polyamide 66 (PA66) physically differ in terms of melting point, glass-transition temperature, crystallization, and tensile modulus, among other things. The crystal structure of PA66 is triclinic whereas PA6 has a monoclinic structure, and its tensile modulus is around 2.9 GPa, whereas it is a little lower for PA6. It has been found that for the melt-mixed blends, the presence of PA66 in PA6/PA66 blends leads to a slight increase in the strength but a decrease in the elongation at break.[1] Some of these differences can be traced to the difference in symmetry of their repeat units and to the difference in configuration of functional units at the chains ends. PA6 generally has one amine and one carboxylic acid group at the end of each chain, whereas PA66 contains a mixture of chains that have only amines, only acid groups, or a combination of the two at their ends. Reports in the literature have shown that the differences in end group configuration can lead to significant differences in the morphology and properties of blends with functionalized polymers made from the two materials.[2–4]

The blending of two or more polymers results in more diversified morphologies, and the compatibility between the components determines their distribution in the system. The interchange reactions can promote the compatibility of the blends.[5] If only the transreacion between the components in the polyamide blends is concerned, increasing temperature and time of mixing or annealing could enhance the transamidation reactions and shorten the segment length.[6,7] Generally, during the interchange reaction, block copolymers form in the initial stages and change to random copolymers if the reaction proceeds for a longer time.[6] However, it is believed that such transamidation takes place at a low rate.

For a dispersed clay structure both the interactions and the interfacial tension between the dispersed component and the matrix are deserved to care. The addition of a third polymeric component, either partially miscible or one that interacts or that reacts with the two components of the blends, has been used successfully.[8–11] This can also be used in the case of the matrices where clay exfoliation is difficult. In our work PA6 is both miscible in PA66 and

Correspondence to: W. Wu (wuwei@ecust.edu.cn).

able to exfoliate organic modified montmorillonite (OMMT) in the melt state. So it could be used to exfoliate OMMT and then produce PA66-rich nanocomposites by mixing with PA66 in two stages.

In the polymer-based composites the presence of reinforcement improves the elastic modulus without worsening the rheological and optical properties of the polymer matrix. The extent of improvement is determined by the reinforcement effect and by the microstructure represented by the size, shape, and homogeneity of the reinforcement. Recently, researches on these materials have generally indicated that polymer-based nanocomposites exhibit improved properties, which are not displayed in the dual phases by their macro and microcomposite counterparts.[12] This was generally attributed to the large specific surface area of the nano-scale reinforcement. Also, physical properties, such as surface smoothness and barrier properties, cannot be achieved by using conventional micrometric reinforcements.[13–15]

A significant drawback of polymeric silicate nanocomposites that limited their vast range of potential engineering applications is reduced toughness, especially when the OMMT content was above 5 wt %,[16,17] despite the large improvement in elastic modulus. Recently, much attention was paid to improve the toughness of polymer/clay nanocomposites and the effects of particle size, interparticle distance and concentration were studied.[16,18,19]

Maleic anhydride-grafted polyethylene-octene copolymer (POE-*g*-MA), a kind of elastomer, used as the toughening agent. Fracture toughness of nylon 6/OMMT nanocomposite is significantly improved by adding POE-*g*-MA particles. Internal cavitation of POE-*g*-MA particles leading to effective relief of crack-tip triaxial stress along with craze-like damage features consisting of line arrays of expanded voids was observed. Subsequently, large scale yielding of nylon 6 matrix and stretching of elastomer particles were facilitated in the crack tip region. These deformation and failure mechanisms are the primary origins of the large toughness of these ternary nanocomposites.[20]

In this work, we have tried to obtain POE-*g*-MA toughened PA66/ PA6/OMMT nanocomposites rich in PA66 using extruded PA6/OMMT exfoliated nanocomposites as a master-batch through coextruding on a twin-screw extruder and the subsequent injection molding. The morphologies obtained were analyzed by X-ray diffraction (XRD), scanning electron microscopy (SEM), and transmission electron microscopy (TEM). The thermal properties of the nanocomposites was characterized by differential scanning calorimetry (DSC) and thermogravimetric analysis (TGA), and the mechanical properties were measured by means of tensile, flexile, and impact tests. The effect of elastomers reinforcement and blending sequence (which influences the microstructure) on crystallization, and mechanical properties were also investigated at the micro and nano-scales.

EXPERIMENTAL

Materials and preparation of nanocomposites

The Polyamide 6,6 was EPR27 (Shenma Nylon Engineering Plastic, Pingdingshan, China) and the Polyamide 6 was YH800 (Baling Petrochemcial, Yueyang, China). The filler was a natural surface-modified montmorillonite (DK5, a nanometer montmorillonite including calcium, sodium, sodium-calcium, magnesium smectite, the average crystal thickness is less than 25 nm, the content of montmorillonite is higher than 95%. Zhejiang Fenghong Clay Chemicals, Anji, China) (OMMT). The toughenners were POE-*g*-MA (CMG9805, MAH: 0.8%, Shanghai Sunny New Technology Development, Shanghai, China) and ABS (747S Taiwan Qimei, Taiwan). Antioxidant agent (Irganox 1010, Ciba) and White Oil were also added as indispensable additives.

Drying before processing was performed at 90°C *in vacuo* for 14 h for PA66 and PA6, and at 80°C in an air-circulation oven for 4 h in the case of OMMT. The 90/10 wt/wt PA6/OMMT nanocomposite master-batch was obtained in a TE-20 corotating twin-screw extruder. The diameter and length to diameter range of the screws were 21.7 mm and 32, respectively. The barrel temperature was 240°C and the rotation speed was 150 rpm. After extrusion, the extrudate was cooled in a water bath and pelletized. It is known that PA6/OMMT master-batches with large OMMT contents are not well exfoliated.[21,22] The elastomers toughening PA66/PA6/OMMT nanocomposites with OMMT contents up to 3 wt % were obtained in the twin-screw extruder at a barrel temperature of 275°C and a rotation speed of 70 rpm. The compositions (wt) of the PA66/PA6/OMMT/POE-*g*-MA obtained were 80/9/1/10, 70/18/2/10, and 60/27/3/10. For comparison, ABS was also used as a toughener in a content of 10 wt %. Subsequent injection molding was carried out in a CHEN DE CJ80M2 B-II Plastics screw injection molding machine to obtain tensile (GB/T1040-92), flexile (GB1042-79) and impact (GB1043-79) specimens. The screw of the plasticization unit was a standard screw with a diameter of 18 mm, L/D ratio of 17.8 and compression ratio of 4. The melt temperature was 275°C. The injection speed and pressure were 11.5 cm^3/s and 2300 bar, respectively.

Morphology characterization

X-ray diffraction patterns were recorded in a Japan Rigaku D/max 2550VB/PC X-ray diffraction system

at 40 kV/100 mA, using a Ni-filtered Cu-Ka radiation source. The scan speed was 0.58°/min. Blend morphology was examined using a JSM-6360 Keck Field Emission SEM and a Hitachi H-800 electron microscope at an acceleration voltage of 200 kV. Samples for the SEM were fractured under liquid nitrogen and then coated with Au/Pd. Samples for TEM were sectioned from molded dog bones and ultrathin-sectioned at 60–100 nm using an ultramicrotome (Reichert-Jung, ultracut E).

The measurement of particle size distribution

Rubber particle size analysis was performed using the image measuring and processing software PSD Calculation, developed by Fudan University in China. Because most of the rubber particles are sphere in shape, the diameter of rubber particles in the TEM micrographs was measured and their averages were calculated. Typically over 200 particles and several fields of view were analyzed.

Mechanical characterization

Tensile testing was carried out using an SANS extensometer at a cross-head speed of 10 mm/min and at 23 ± 2°C and 50 ± 5% relative humidity. The mechanical properties, such as tensile strength and ductility, were determined from the load–displacement curves. Izod impact tests were carried out on notched specimens using a XCJ-4 4/1 J pendulum. The notches (depth 2.54 mm and radius 0.25 mm) were machined after injection molding. A minimum of five tensile specimens and 10 impact specimens were tested for each reported value.

Thermal measurement

The thermal properties were studied both by DSC and TGA. The DSC scans were carried out using a CDR–4P DSC calorimeter in a nitrogen atmosphere and using an indium sample as reference. TGA was carried out at a heating rate of 10°C/ min under nitrogen flow of 50 mL/min by a thermogravimetric analyzer SDT Q600 (TA, US).

Rheology measurement

The melt flow index (MFI) of the samples was obtained at 275°C with a load of 325 g (GB3682-83) using an SRSY-1 melt flow indexer. Dynamic rheological and steady-state shearing measurements were conducted with a Rheo Stress (RS 600) Rheometer (HAAKE, Germany) using a parallel plate system with plate of diameter 20 mm. Samples were dried for 10 h in a vacuum dryer at 90°C, and the rheometer was purged with dry nitrogen throughout the test. Frequency range from 10^{-2} to 10^{2} Hz and shear rate range from 0.01 to 100 1/s were used for dynamic and steady-state tests, respectively. Storage (G') and loss modulus (G'') were monitored in the linear-viscoelastic region. 260°C was taken as the reference temperature.

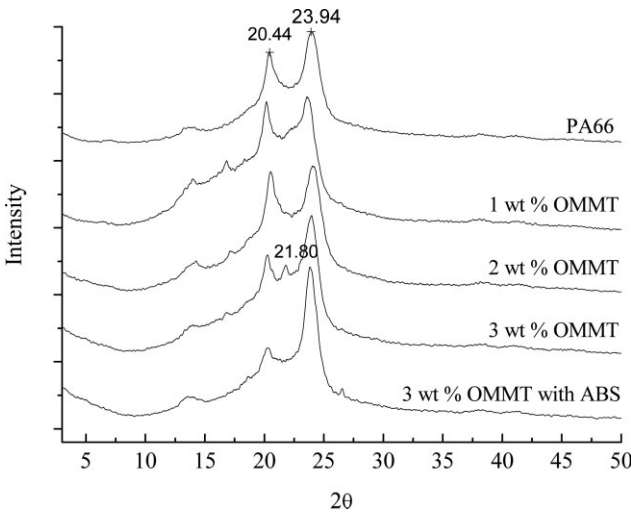

Figure 1 X-ray diffraction patterns of pure PA66 and the POE-*g*-MA (ABS) toughened PA66/PA6 nanocomposities with 1–3 wt % OMMT.

RESULTS AND DISCUSSION

Crystallization characterization of the nanostructure

The crystal structures observed in polyamide mainly falls into two categories: α crystalline phase and γ crystalline phase. Injection-molded PA6 consists of a mixture of α and γ phases, but upon OMMT addition PA6 preferentially forms the γ phase. The diffraction peaks at $2\theta = 19.5°$ and 23.5° correspond to the α phase, whereas that at $2\theta = 21°$ corresponds to the γ phase. In the blend nanocomposite, the OMMT in the PA6 matrix acts as a nucleating agent stabilizing the γ crystalline form of PA6 similarly to the OMMT in the homopolymer. PA66 has various crystalline phases and usually presents the more stable α phase rather than the γ phase in XRD pattern. Two strong diffraction peaks at $2\theta = 20.4°$ and 24.1°, which are assigned to (100) and (010, 110) crystal planes respectively,[23] are distinctive features of the α-form crystal of PA66, and can be indexed by a simple one-chain triclinic unit cell.

As OMMT interacts favorably with PA6 and PA66, PA6 and PA66 are miscible and can be blended into a phase. It is expected that the alloy would display the same polymorphism behavior as previously reported in nylon nanocomposites.

Figure 1 shows the XRD patterns of pure PA66 and the POE-*g*-MA (ABS) toughened PA66/PA6

nanocomposites samples, which were slowly cooled to room temperature naturally after being melted into thin films at 280°C. The two strong diffraction peaks at $2\theta = 20.44°$ and 23.94° are the distinctive feature of the α phase of PA66, which are designated as α1 and α2, respectively. When adding 1 wt % OMMT, the XRD pattern still shows only the presence of the α phase, however, the spectra of the nanocomposite presents peaks left shift slightly in comparison with those of pure PA66, indicating that the new diffraction peaks of PA6 have been overlapped upon the old diffraction peaks of PA66 and PA6 has some influence on the crystalline morphology of PA66 over the loading level examined. When adding 3 wt % OMMT, the intensities of the α1 and α2 peaks have changed greatly. The α1 peak is notable in pure PA66, whereas the α2 peak is much higher than the α1 peak in the nanocomposite with 3 wt % OMMT. More OMMT loading induces the variation in crystal structures and a new little diffraction peak appears in the nanocomposites with 3 wt % OMMT. The characteristic of the γ phase is the new diffraction peak at $2\theta = 21.7°$; the small diffraction peak at $2\theta = 13.6°$ overlapped by that of pure PA66 is also contributed by the γ phase; they are designated as γ1 and γ2, respectively. In addition to the observation of the γ phase, in sharp contrast to PA66, the α1 diffraction peak diminishes greatly in the nanocompositie with 3 wt % OMMT and the ABS toughened nanocomposites. One can draw the following conclusions from above results: the introduction of silicate layers with PA6 induces the appearance of the γ crystal phase in the nanocomposites, which is unstable and seldom appears in PA66 at room temperature; the addition of OMMT also changes the structure of the α crystal phase.

The α phase consists of planar sheets of hydrogen bonding chains with sheets stacked upon one another and displaces along the chain direction by a fixed amount. The γ phase has pleated sheets of methylene units with hydrogen bonding between sheets rather than within sheets. The principal structural difference between α and γ phase is that the amide-to-methylene dihedrals are near trans (164–168°) in α and nearly perpendicular to the peptide plane (∼ 126°) in γ phase.[24–27] The sharp decrease in intensity of the α1 peak in the nanocomposites indicates that the addition of OMMT disturbs the perfect arrangement of hydrogen bonded sheets of the α phase. This result also verifies the explanation to the appearance of the γ phase in the nanocomposites with 3 wt % OMMT.

Vaia and coworkers[28] suggest that the proximity of the surface of layers results in conformation changes of chains, limiting the formation of hydrogen bonded sheets of the α phase, which can be verified by our above result that the α1 diffraction peak diminishes greatly in the nanocomposites, coordinating with the amide groups and forcing them out of the plane formed by the chains thus leading to the appearance of the γ crystalline phase. However, the α phase of PA66 is much more thermodynamically stable than that of PA6 at room temperature,[27] that is the reason why the introduction of silicate layers results in just the appearance of γ phase in PA66 but the domination in PA6. The increase of the PA6/OMMT masterbatch, that is, the increase in PA6 loadings and OMMT loadings (the surfaces of layers), would increase the effective influence areas, thus more γ phases are induced from PA6 and appear in the PA66/PA6 alloy.

In addition, no visible diffraction peak normally for OMMT at small angles from 3° to 10° in XRD pattern above is found, which could be attributed to the formation of swollen and disordered intercalated tactoids or the exfoliation of OMMT. As the incorporated amount of POE-*g*-MA was limited, leading to no extra observable diffraction peaks for the blends, no clear effect of this elastomer on the crystalline structure of nanocomposites has been observed. A similar finding is also reached for the ABS cases. In PA66/PA6/ABS nanocomposites either forming a discrete phase or locating at the interface of the matrix and the SAN of ABS, OMMT does not disrupt the phase formation of nanocomposites, which results in a similar crystalline structure as in the unmodified blends.

Morphology

From the SEM photograph of the fracture surface of this blend nanocomposite [Fig. 2(a)], only one matrix phase can be found in PA6/PA66 alloy, which indicates a good miscibility between PA6 and PA66 when the loading of PA6 is in the range of 0–40 wt %.

As POE-*g*-MAH is easy to be grafted to the matrix because of the *in situ* formation of PA66-*co*-POE-*g*-MA copolymer, which helps in fine dispersion of POE-*g*-MA in the PA66 matrix with good interfacial interaction, in the SEM photograph Figure 2(b), the improvement in the interfacial adhesion can be found as the elastomers only were presented as some flurry domains in the matrix and show practically some debonding.

In the TEM photograph of PA66/PA6/POE-*g*-MA nanocomposites with 3 wt % OMMT (In Fig. 3, white sphere zones represent POE-*g*-MAH domains.) one can observe that most of elastomers are surrounded by the exfoliated OMMT, and the OMMT layers or strips are spread from the elastomer as a core to stretch out deeply into the matrix. It is easy to imagine that the OMMT strips in the hedgepig-shape structure can deliver the stress from the

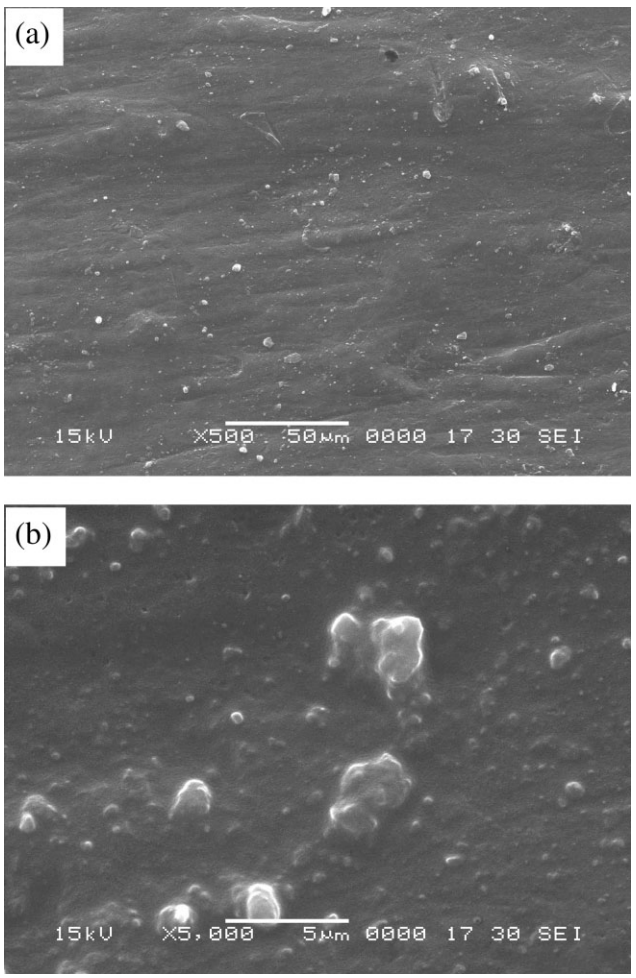

Figure 2 SEM photographs of the fracture surface of PA66/PA6/POE-*g*-MA nanocomposites with 3 wt % OMMT, (a) at magnification of ×500, (b) at magnification of ×5000.

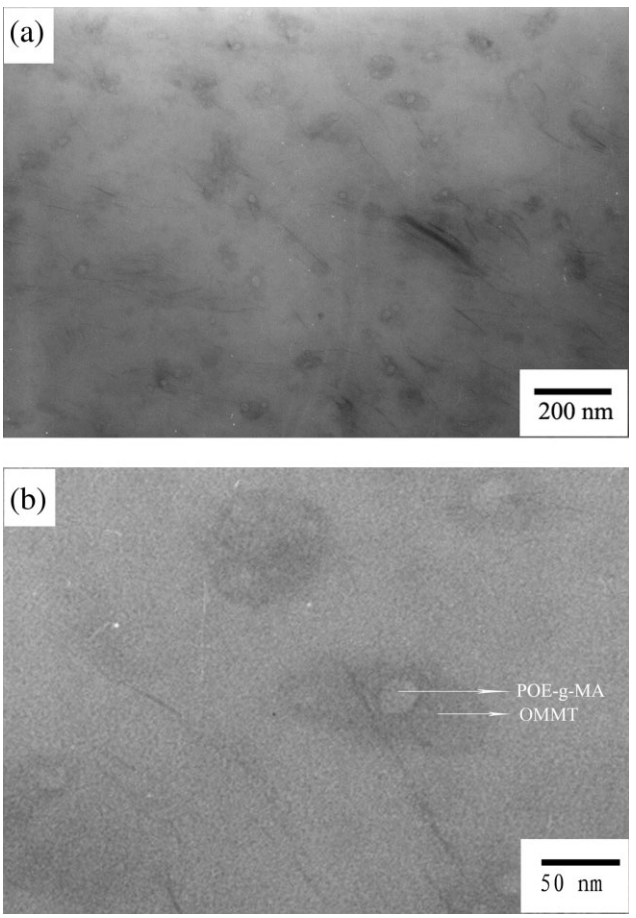

Figure 3 TEM photographs of PA66/PA6/POE-*g*-MA nanocomposites with 3 wt % OMMT.

elstomers into the matrix in all directions and can dissipate the energy effectively. Schematic diagram of the hedgepig-shape structures can be seen in Figure 4. Perhaps the forming of the hedgepig-shape structures attributes to the following course: the formation of PA6 phase and OMMT network took place earlier than the melting of PA66 and POE-*g*-MAH. Once the exfoliated OMMT layers existed in the continuous PA66/PA6 alloy phase, the coalescence of the dispersed POE-MAH would be blocked or locked even after the melting of POE-*g*-MAH. On the other hand, the elastomers particles seem to affect the alignment of OMMT layers in the immediate vicinity because of the interaction between the maleic anhydride groups of POE-*g*-MA and hydroxyethyl groups of OMMT, which would accelerate the exfoliation of OMMT in further.

Since the OMMT was firstly exfoliated in PA6, it can be imagined that some pure PA6 still remained in the intercalated OMMT layers of the hedgepig-shape structures because of the melt flow resistance, that is, there are more contents of PA6 in the special structure compared with the matrix. Furthermore more PA6 in it with lower crystallization rate compared with PA66 brings more amorphous regions in it, taking it into consideration that the amorphous region is responsible for nearly total of the elastic deformation under stress. In addition, for the scarce

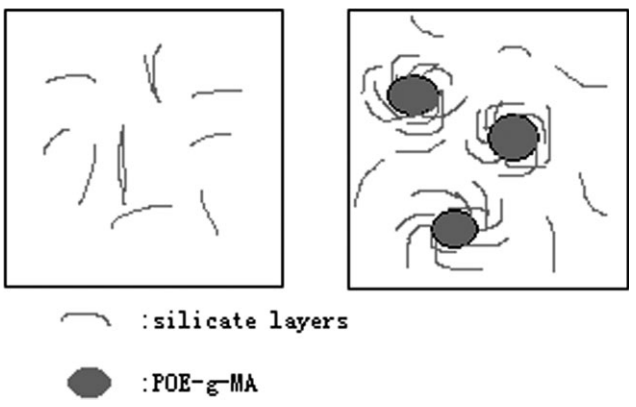

Figure 4 Schematic diagram of the hedgepig-shape structures.

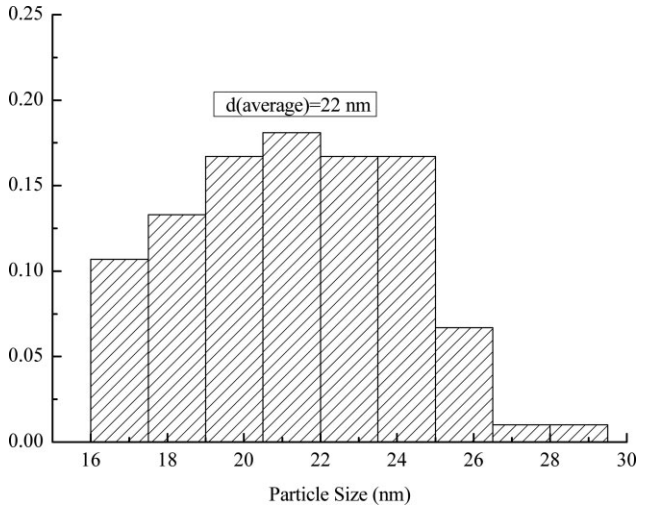

Figure 5 The particle size distribution of rubber in TEM photographs of PA66/PA6/POE-*g*-MA nanocomposites with 3 wt % OMMT.

crystalline phase in the special structure the existence of PA6 results in an increase of γ crystal and the formation of fine spherulites. The presence of γ crystals inhibits the crystallographic slip, and the lamella in the blends would become thicker because of the OMMT as nucleating agent, these are detrimental to toughness. Although altogether the mobility of kinetic elements taking part in a plastic deformation is still higher, and as a result, the energy dissipated increases and a large deformation is produced in the hedgepig-shape structures.

The presence of OMMT simultaneously in the matrix and the interface is unusual. This dual positioning indicates two roles for the OMMT layers: one as a compatibilizer being shared by both polymers to reduce the interfacial tension, resulting in smaller POE-*g*-MAH domains, which seem to toughen the blends better. And the other as a nano-filler, because PA66 is more polar than POE-*g*-MA, the OMMT exhibits fully exfoliated structure in the PA66 matrix, so the presence of the OMMT can stabilize the different polymer crystalline phases and improve some mechanical properties as will be discussed in the following paragraphs.

Domains size

The size of the domains becomes much smaller than any of one batch blends as determined from TEM imaging. The analysis of particle size distribution is also done in Figure 5. The dispersion of POE-*g*-MA particles is fine and homogeneous; the mean particle size of which is 22 nm.

It is indicated earlier that PA66-*co*-POE-*g*-MA copolymer formed *in situ* during the melt extrusion of PA66 and POE-*g*-MA improves the compatibility between PA66 and POE-*g*-MA by lowering the interfacial tension, and thus decreases the sizes of POE-*g*-MA particles.

From the viewpoint of OMMT, in the (PA6/OMMT)/PA66/ POE-*g*-MA sequence, during the fabricating of PA6/OMMT master-batch, OMMT has been well exfoliated, when to the final (PA6/OMMT)/PA66/ POE-*g*-MA blending, perhaps the well exfoliated OMMT in the melt would take stronger influence on the melt elastomers than that in one batch process. It can be easily imagined that the well exfoliated OMMT layers as many small obstacles retard the rate of coalescence of a dispersed polymer phase seriously during the whole blending course. Thus, the elastomers particles in the alloy nanocomposites would be smaller in size when compared with the neat nylon.

Controlling the domain size is crucial as the amount of crystallization scales with domain size. In a polymer blend, which is essentially a mix of two viscous, incompressible fluids, domain size is related to the breakup of threads (surrounded by matrix) into droplets because of Rayleigh instability.[29] Empirically, domain size (A_n) has been determined to depend on the interfacial tension (γ), the viscosity ratio of the dispersed phase to the matrix phase (η_d/η_m), the shear rate (G), and the melt viscosity (η_{me}) as shown in the following equation.[30]

$$A_n = 4[\eta_d/\eta_m]^k \gamma/(G\eta_{me}) \quad (1)$$

where $k = 0.84$ for $\eta_d/\eta_m \geq 1$ and $k = -0.84$ for $\eta_d/\eta_m \leq 1$. The equation implies that the smallest domains are generally the result of a viscosity ratio that is close to unity. For the blends studied in this work where POE-*g*-MA is the domain phase and the alloy is the matrix phase, the viscosity ratio is less than unity.[31]

For the blends in the current study, the shear rate (G) is held constant as the blends are all extruded at the same rate. Compared with the common one batch blends, the viscosity ratio is on the same level. So the variable changes can only be the melt viscosity and the interfacial tension. The viscosity of the final (PA6/OMMT)/PA66/POE-*g*-MA blending melt is larger than that of the common OMMT blend melt in one batch because OMMT has been well exfoliated before blending (Fig. 11), thus, from the equation aforementioned it is reasonable for the domains size to become smaller than that in one batch. Furthermore, it can be expected that the interfacial tension is lowered in some degree because of the presence of PA66-*co*-POE-*g*-MA copolymer, which can improve the compatibility between PA66 and POE-*g*-MA. From the equation aforementioned we

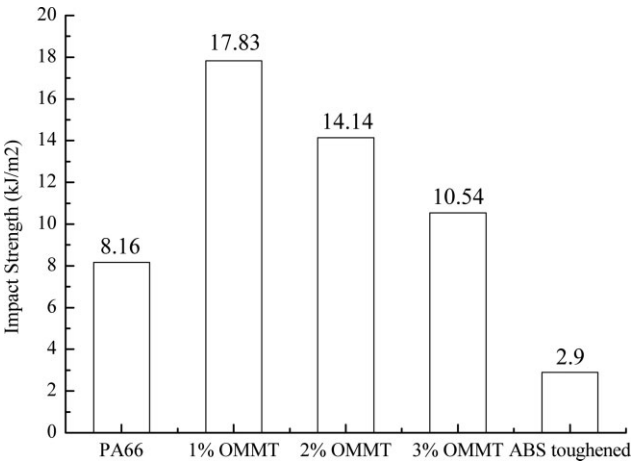

Figure 6 The comparison of the Izod impact strength values for pure PA66 and the POE-*g*-MA (ABS) toughened PA66/PA6 nanocomposities with 1–3 wt % OMMT.

can get the other reason for the smaller size of elastomers.

Impact behavior

In general, the effective mechanisms of energy absorbing are needed to increase the toughness of a given material. For unreinforced thermoplastics, crazing and shear yielding are the two frequently encountered energy absorbing mechanisms.[32] Conversely, for polymer based micrometric and nanometric composites, in their recent work, Thio et al.[33] have shown that debonding of reinforcement is an important mechanism in promoting fracture toughness of polymer-matrix based composites as it allows plastic stretching of polymer ligaments between the debonded particles. The elastomers like POE-*g*-MA can support the debonding mechanism because *in situ* formation of PA66-*co*-POE-*g*-MA copolymer improves the interfacial adhesion between elastomers particles and matrix. So POE-*g*-MA is expected to be an ideal elastomer to toughen the present nanocomposites.

The rubber particle size or interparticle distance plays a key role in toughening of plastic materials as suggested by Wu.[34] The lower and upper limits of the weight-average diameter of rubber particles were shown to be 0.1 and 1 μm for nylon 6 by Oshinski et al.[35] Although these limits may be different if we regard the matrix as the nanocomposite. It is expected that by reducing the POE-*g*-MA particle size in final blends or even finer, significant improvement in impact toughness can be achieved along with other mechanical properties.

The Izod impact strength values for pure PA66 and the POE-*g*-MA (ABS) toughened PA66/PA6 nanocomposites with 1–3 wt % OMMT are summarized in Figure 6. For the POE-*g*-MA toughened series, the addition of elastomer causes a large increase in the Izod value as expected, while the impact strength decreases step by step with the increasing of OMMT loading. To understand the effects shown here, it is important to remember that the Izod value is the area under a force–displacement curve. As the addition of OMMT reduces the extent of plastic deformation, that is, reduces the area under a force–displacement curve at least in tensile tests as shown in Figure 7. The better properties of nanocomposites with more loading of OMMT are also expected in the future studies.

Tensile and flexile properties

The addition of OMMT clearly increases Young's modulus and tensile strength but decreases ductility and fracture toughness of nanocomposites. On the other hand, the toughness can be easily improved by using maleated elastomers, such as POE-*g*-MA,[3] whereas the stiffness and tensile strength decrease markedly because of the incorporation of the low modulus elastomer at the same time. All together, we expect to obtain balanced toughness and stiffness of PA66/PA6 nanocomposites by using POE-*g*-MA as a toughener and OMMT as a stiffening and strengthening agent.

One of the ultimate purposes for polymer blending and compatibilizing is to improve mechanical properties. If in fact there is compatibilization, the blend should exhibit improved mechanical properties. Figure 7 shows the representative tensile stress/strain curves for pure PA66, PA66/POE-*g*-MA (90/10 wt %) and the nanocomposites with 1–3 wt % OMMT. As expected the tensile strength decreases

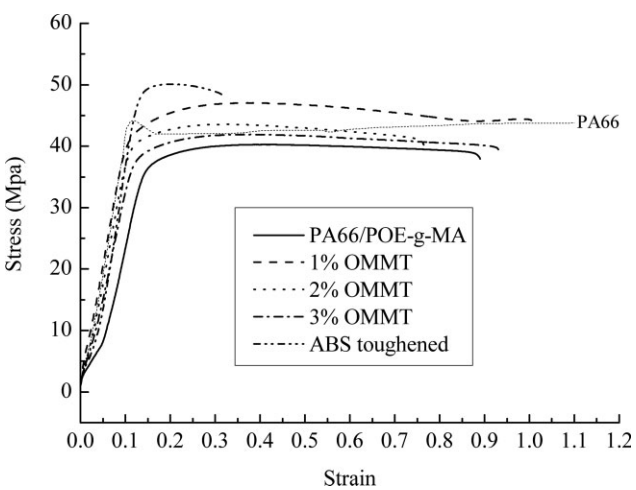

Figure 7 Tensile stress–strain curves for pure PA66, PA66/POE-*g*-MA (90/10 wt %) and the POE-*g*-MA (ABS) toughened PA66/PA6 nanocomposities with 1–3 wt % OMMT.

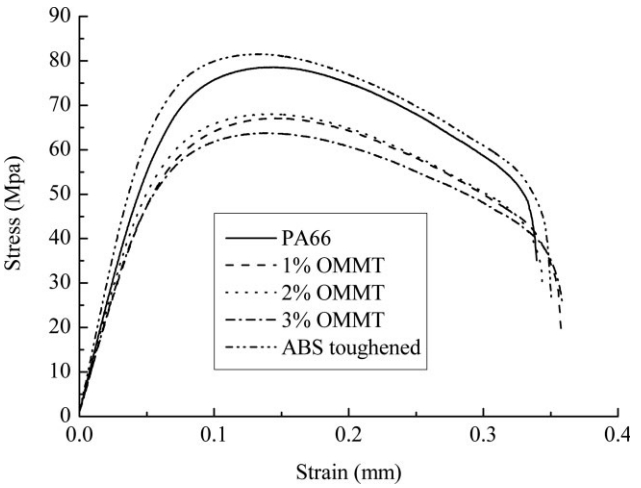

Figure 8 Flexile stress–strain curves for pure PA66 and the POE-*g*-MA (ABS) toughened PA66/PA6 nanocomposities with 1–3 wt % OMMT.

on addition of the elastomer but increases on addition of OMMT. With as little as 1 wt % OMMT, the tensile properties of the nanocomposite are improved remarkably compared with the PA66/POE-*g*-MA blend. Not only are the nanocomposites stiffer but they also show higher strength. The addition of both elastomer and well exfoliated OMMT has compensating effects on the tensile properties that more or less parallel the trends of adding just elastomer as seen in Figure 7.

Compared with POE-*g*-MA, ABS-toughened nanocomposite exhibits worse toughening but a better flexile properties as seen in Figure 8, which indicates the excellent flexile resistance of ABS. Furthermore, from the Figure 7 on tensile stress/strain curve, ABS-toughened nanocomposite shows a better tensile strength and Young's modulus with a very bad elongation at break at the same time. All above express that ABS is a stiffer toughener than POE-*g*-MA.

Thermal properties (DSC and TGA)

To better reveal the effect of OMMT loading, Table I listed DSC thermal analysis of PA66/PA6/POE-*g*-MA nanocomposites with 1–3 wt % OMMT. Strictly speaking, the effect of OMMT on the melting temperatures under 10°C/min heating condition was comparatively limited, whereas the heat of fusion decreases with the increasing of PA6/OMMT loading, which was probably ascribed to the increasing of exotic uncrystallized OMMT and more imperfections in the crystalline structures resulting from the well exfoliated silicate layers of OMMT penetrating into the α crystal phase of PA66 and the disturbing effect of the different crystal lattice of PA6 in the PA66 matrix.

PA66 has a melting point of 262°C, which is higher than that of PA6 at 219°C. From the DSC curves of PA66/PA6/POE-*g*-MA nanocomposites (Fig. 9), the melting points of nanocomposites with 1–3 wt % OMMT shown in Table I can be gotten. The relatively lower melting points of nanocomposites compared with pure PA66 may attribute to the introduction of PA6 with a much lower melting points in the PA66/PA6 systems.

The TGA curves of the PA66/PA6/POE-*g*-MA nanocomposites with 1 wt % OMMT and 3 wt % OMMT in nitrogen atmosphere are shown in Figure 9. It is obvious that the two curves are so similar that they are nearly overlapped with each other. The decomposition temperatures of them are also similar and beyond 400°C. However, the nanocomposites have lower decomposition temperatures than pure PA66 (424°C). It may be due to the catalysis of water in OMMT (bound or from dehydroxylation).[36] Except that no clear influence of PA6 loading can be found on the high temperature resistance of the nanocomposite compared with pure PA66. So the PA66/PA6/POE-*g*-MA nanocomposites still maintain a very good thermal stability.

Rheology properties

Figure 10 shows the Melt Flow Index (MFI) valves of pure PA66 and different rubbers toughened nanocomposite with different OMMT contents. It can be observed that the MFI valves of nanocomposites after the introduction of OMMT are much smaller than that of pure PA66. It is interesting to note that the MFI value of the nanocomposite with relatively high loading of PA6 is significantly higher compared with that of the low PA6 loading. As for ABS toughened nanocomposite, the higher MFI valve indicates that the styrene with a low melt viscosity in ABS takes a more active effect on melt viscosities of the nanocomposite compared with the elastomer POE-*g*-MA.

The trend of the MFI values reflects two opposing phenomena. In the beginning, the addition of OMMT tends to increase the matrix melt viscosity

TABLE I
DSC Thermal Analysis of PA66/PA6/POE-*g*-MA Nanocomposites with 1–3 wt % OMMT

		PA66/(PA6/OMMT/POE-*g*-MA		
Sample	Pure PA66	1% OMMT	2% OMMT	3% OMMT
T_m (°C)	262.7	261.4	259.6	259.3
ΔH_m (J/g)	45.32	36.32	29.11	28.29

T_m: melting temperature.
ΔH_m: Heat of fusion.

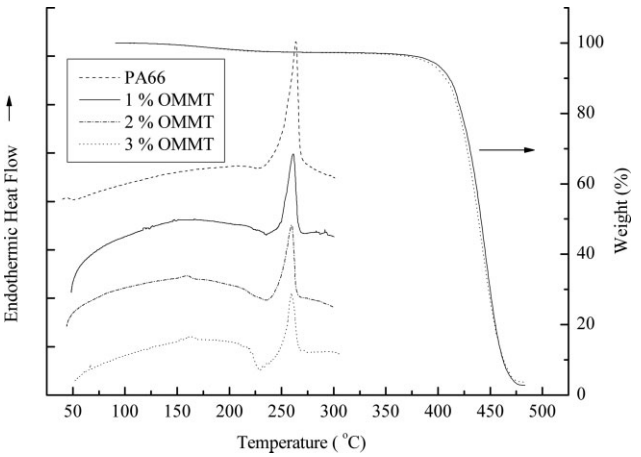

Figure 9 DSC curves and TGA curves of PA66/PA6/POE-*g*-MA nanocomposites with 1–3 wt % OMMT in nitrogen atmosphere.

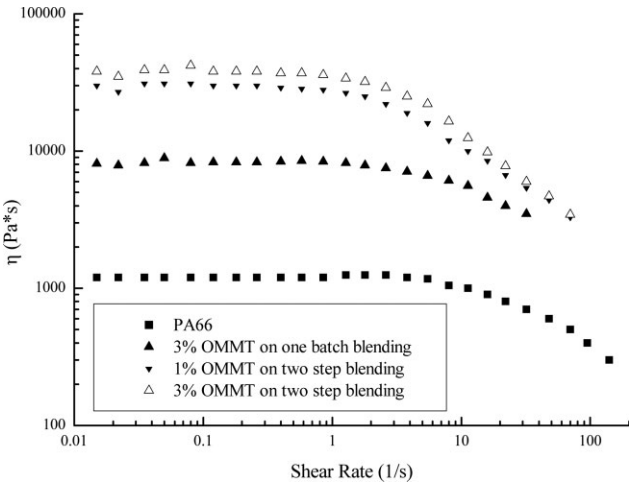

Figure 11 The steady shear viscosity as a function of shear rate for pure PA66 and the POE-*g*-MA toughened PA66/PA6 nanocomposities with 1–3 wt % OMMT on one or two step blending.

and thus make the MFI valves lower; however, the degradation of the organic component of OMMT leads to the degradation of the matrix molecule, especially for the PA6 of the nanocomposites in relatively higher processing temperature (275°C), which increases the MFI valves as recently described by Fornes et al.[37] With more OMMT loading, the viscosity effect of matrix degradation apparently exceeds the intrinsic increase caused by the addition of OMMT, thus, pushing the MFI values higher.

On the other hand, PA6 and PA66 have different melting temperatures and are generally extruded at 240°C and 270°C, respectively. The torque values for the two polymers are very similar at 270°C, which suggest that comparisons of nanocomposites formed from PA6 and PA66 at this temperature would be relatively free of any differences because of melt viscosity effects.[38]

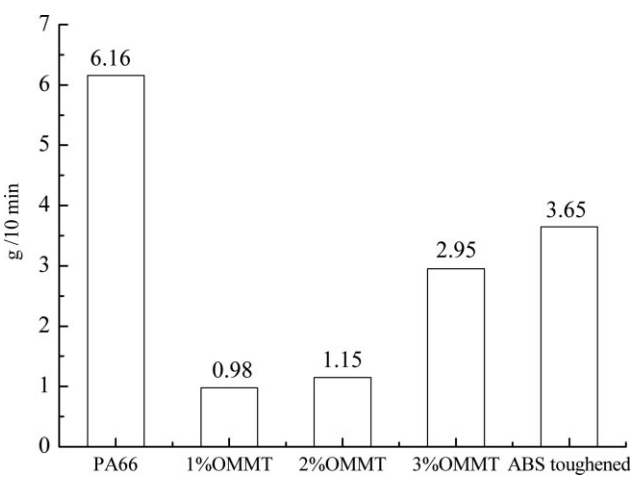

Figure 10 The comparison of Melt Flow Index (MFI) valves of pure PA66 and the POE-*g*-MA (ABS) toughened PA66/PA6 nanocomposities with 1–3 wt % OMMT.

In our studies, with the increasing of PA6 loading, MFI valves of the nanocomposite increase sharply. Because the POE-*g*-MA loading is in the same level, so the key factor is just the higher loading of PA6. Although it is totally miscible between PA66 and PA6, some unexpected phenomena still happens, for example, the melt temperatures of the blend would be lower even than that of pure PA6 when PA66 loading gets into the range of 45–55% in the PA66/PA6 blend.[39] By assuming that the high loading PA6 can lower the blend melt temperature remarkably, which would be in favor of decreasing the melt viscosity in relatively higher processing temperature, then MFI valves of the nanocomposite can be said to increase with the adding of PA6 loading. Whereas from the viewpoint of inner structure, perhaps the high loading PA6 can act as a good lubricant to decrease the melt viscosity efficiently in the melt PA66/PA6 blend.

The steady shear viscosity as a function of shear rates for PA66 and its nanocomposites is shown in Figure 11. It can be seen that the viscosities of the nanocomposites are much higher than that of neat PA66 and an independent viscosity plateau at lower shear rates and shear thinning at higher shear rates are shown on each curve. The phenomenon above is very similar to that of the other kinds of OMMT nanocomposites.[40,41] For the exfoliated nanocomposites (with 1 and 3 wt % OMMT loading), the viscosities increase slightly with increasing the OMMT loading, which is quite similar to the case of the dynamic complex viscosity (Fig. 12) . However, the steady shear viscosity of the nanocomposite with 3 wt % OMMT loading in two step blending is several times of that of the nanocomposite in one batch blending in the range of 0.01–1.0 1/s, which should

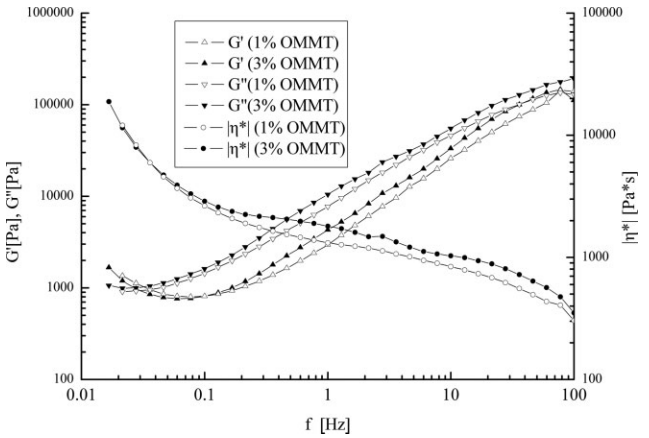

Figure 12 Dynamic rheology curves of the POE-*g*-MA toughened PA66/PA6 nanocomposites with 1 and 3 wt % OMMT at 260°C: Storage modulus (G'), Loss modulus (G'') and complex viscosity $|\eta^*|$ as a function of frequency, respectively.

attribute to the different exfoliating level of OMMT layers.

The viscoelastic response as measured by the storage and loss modulus (G' and G'') for the nanocomposite with 1 and 3 wt % OMMT is shown in Figure 12. G' and G'' represent the elastic and viscous responses of the studied system, respectively. It is clearly seen that the nanocomposites with various loading of OMMT display an increase in both elastic and viscous response with increasing frequency. The frequency dependence of G' and G'' shows that the G'' value is a little bigger than the G' value, indicating that the nanocomposites exhibit viscoelastic liquid characteristics under shear. On the other hand, for both nanocomposites, two intersections of the G' and G'' curves at lower and higher frequencies are observed as shown in Figure 12. The intersections are usually associated with the transition from the plateau zone to terminal region of the polymers or reverse, which indicates that the nanocomposites are changing the rheological behavior from a viscoelastic liquid (where $G' < G''$) to a viscoelastic solid (where $G' > G''$) and become more elastic.[42]

Figure 12 also exhibits the dynamic complex viscosity $|\eta^*|$ as a function of frequency. It can be seen that the two nanocomposites exhibit rheological behavior of non-Newtonian fluids, as indicated by the decrease of their steady shear viscosities with the increasing of shear rates. Perhaps the decrease in viscosity with increase in frequency for the nanocomposites is because of the preferential adsorption of higher molecular mass fraction of the blend at the filler surface.[43] At low frequency, the network structure of the OMMT is not disrupted; however, with the increasing of frequency, the secondary forces between silicate layers can be broken, and the viscosity decreases markedly.

CONCLUSIONS

In this study, elastomers toughened PA66/PA6 nanocomposites were examined in terms of impact, tensile, and flexile properties. Several different compositions varying in the content of OMMT, different kinds of rubbers were prepared by mixing PA6 with MMT as a master-batch in a twin screw extruder and then blending PA66 and the master-batch with the elastomers in a twin screw extruder. In this sequence, the MMT platelets were efficiently dispersed in the nanocomposites matrix.

There are two effects of OMMT layers on crystallization of the nanocomposites: (1) the introduction of silicate layers with PA6 induces the appearance of the γ phase in nanocomposites which is unstable and seldom appears in PA66 at room temperature; (2) constraining the motion of chains that hinders of the refinement of the α crystal structures.

Most of elastomers in the nanocomposites are surrounded by the exfoliated OMMT and the OMMT strips are spread from the elastomers as a core to stretch out deeply into the matrix. The OMMT strips in the hedgepig-shape structure can deliver the stresses from the elstomers into the matrix in all directions and can dissipate the energy effectively.

PA66-*co*-POE-*g*-MA copolymer formed *in situ* during the melt extrusion of PA66 and POE-*g*-MA improves the compatibility between PA66 and POE-*g*-MA by lowering the interfacial tension, and thus decreasing the sizes of POE-*g*-MA particles. The smaller POE-*g*-MAH domains seem to toughen the blends.

For the elastomer toughened series, the addition of elastomer causes a large increase in the Izod impact strength value as expected, whereas the impact strength decreases step by step with the increasing of MMT loading. The tensile strength decreases on addition of the elastomer but increases on addition of OMMT. Compared with the PA66/POE-*g*-MA blend, the tensile properties of the nanocomposites are improved remarkably. Not only are the nanocomposites stiffer, they also show higher strength. The addition of both elastomer and well exfoliated OMMT has compensating effects on the tensile properties. The better properties of nanocomposites with more loading of OMMT are also expected in the future studies.

Compared with POE-*g*-MA, ABS toughened nanocomposite exhibits worse toughening but better flexile properties, which indicates the excellent flexile resistance of ABS. Although from the tensile stress/strain curve, ABS toughened nanocomposite

shows a better tensile strength and Young's modulus with a very bad elongation at break at the same time. All the aforementioned express that ABS is a stiffer toughener than POE-*g*-MA.

Fusion heat of the nanocomposites decreases with the increasing of PA6/OMMT loading, which is probably ascribed to the increasing of exotic uncrystallized OMMT and more imperfections in the crystalline structures resulting from the well exfoliated silicate layers of OMMT penetrating into the α crystal phase of PA66 and the disturbing effect of the different crystal lattice of PA6 in the PA66 matrix.

The nanocomposites display an increase in both elastic and viscous response with increasing frequency. The frequency dependence of G' and G'' show that the G'' value is a little bigger than the G' value, indicating that the nanocomposites exhibit viscoelastic liquid characteristics under shear. The nanocomposites exhibit rheological behavior of non-Newtonian fluids. At low frequency, the network structure of the OMMT is not disrupted, however, with the increasing of frequency, the secondary forces between silicate layers can be broken, and the viscosity decreases markedly.

In the next studies the relationship of impact strength versus temperature would be examined to determine the ductile–brittle transition temperatures as a function of MMT and rubber contents. In addition, future studies would seek to better understand how the orientation of OMMT layers affects the morphology of rubber phase and the optimum range of rubber particle sizes for toughening.

References

1. Wang, X. C.; Zheng, Q.; Yang, G. S. J Polym Sci Part B: Polym Phys 2007, 45, 1176.
2. Oshinski, A. J.; Keskkula, H.; Paul, D. R. Polymer 1992, 33, 268.
3. Oshinski, A. J.; Keskkula, H.; Paul, D. R. Polymer 1992, 33, 284.
4. Takeda, Y.; Keskkula, H.; Paul, D. R. Polymer 1992, 33, 3173.
5. Stewart, M. E.; Cox, A. J.; Naylor, D. M. Polymer 1993, 34, 4060.
6. Eersels, K. L.; Groeninckx, G. Polymer 1996, 37, 983.
7. Walia, P. S.; Gupta, R. K.; Kiang, C. T. Polym Eng Sci 1999, 39, 2431.
8. Kim, S. W.; Jo, W. H.; Lee, M. S.; Ko, M. B.; Jho, J. Y. Polymer 2001, 42, 9837.
9. Lepoittevin, B.; Pantoustier, N.; Devalckenaere, M.; Alexandre, M.; Calberg, C.; Jérôme, R. Polymer 2003, 44, 2033.
10. Dharaiya, D.; Jana, S. C.; Shafi, A. Polym Eng Sci 2003, 43, 580.
11. Lee, M. S.; Ha, M. G.; Choi, C. N.; Yang, K. S.; Kim, J. B.; Choi, G. D. Polym J 2002, 34, 510.
12. Alexandre, M.; Dubois, P. Mater Sci Eng 2000, 28, 1.
13. Kojima, Y.; Usuki, A.; Kawasumi, M.; Okada, A.; Fukushima, Y.; Kurauchi, T. J Mater Res 1993, 8, 1185.
14. Kojima, Y.; Usuki, A.; Kawasumi, M.; Okada, A.; Kurauchi, T.; Kamigaito, O. J Appl Polym Sci 1993, 49, 1259.
15. Gilman, J. W.; Kashiwagi, T.; Lichtenhan, J. D. SAMPE J 1997, 33, 40.
16. Sheng, N.; Boyce, M. C.; Parks, D. M.; Rutledge, G. C.; Abes, J. I.; Cohen, R. E. Polymer 2004, 45, 487.
17. Yu, Z. Z.; Yan, C.; Yang, M. S.; Mai, Y.-W. Polym Int 2004, 53, 1093.
18. Wu, S. J Appl Polym Sci 1988, 35, 549.
19. Dijkstra, K.; Wevers, H. H.; Gaymans, R. J. Polymer 1994, 35, 323.
20. Lim, S.-H.; Dasari, A.; Yu, Z.-Z.; Mai, Y.-W.; Liu, S.; Yong, M. S. Compos Sci Technol 2007, 67, 2914.
21. Dennis, H. R.; Hunter, D. L.; Chang, D.; Kim, S.; White, J. L.; Cho, J. W. Polymer 2001, 42, 9513.
22. Fornes, T. D.; Yoon, P. J.; Hunter, D. L.; Keskkula, H.; Paul, D. R. Polymer 2002, 43, 5915.
23. Ramesh, C.; Keller, A.; Eltink, S. J. E. A. Polymer 1994, 35, 2483.
24. Kyotani, M.; Mitsuhashi, S. J Polym Sci Part A-2: Polym Phys 1972, 10, 1497.
25. Abu-Isa, I. J Polym Sci A-1: Polym Chem 1971, 9, 199.
26. Hiramatsu, N.; Hirakawa, S. Polym J 1982, 14, 165.
27. Dasgupta, S.; Hammond, W. B.; Goddard, W. A. J Am Chem Soc 1996, 118, 12291.
28. Lincoln, D. M.; Vaia, R. A.; Wang, Z. G.; Hsiao, B. S. Polymer 2001, 42, 1621.
29. Palierne, J. F.; Lequeux, F. J. Non-Newtonian Fluid Mech 1991, 40, 389.
30. Wu, S. Polym Eng Sci 1987, 27, 335.
31. Liu, Z. H.; Marechal, Ph.; Jerome, R. Polymer 1998, 39, 1779.
32. Steger, T. R.; Nielsen, L. E. J Polym Sci Polym Phys Ed 1978, 16, 613.
33. Thio, Y. S.; Argon, A. S.; Cohen, R. E. Polymer 2004, 45, 3139.
34. Wu, S. Polymer 1985, 26, 1855.
35. Oshinski, A. J.; Keskkula, H.; Paul, D. R. Polymer 1996, 37, 4909.
36. Davis, R. D.; Gilman, J. W.; Vanderhart, D. L. Polym Degrad Stab 2003, 79, 120.
37. Fornes, T. D.; Yoon, P. J.; Paul, D. R. Polymer 2003, 44, 7545.
38. Chavarria, D. R. Polymer 2004, 45, 8501.
39. Liu, Z.; Zhang, H.; Yao, L. Process Appl Mod Plast (China) 2002, 2.
40. He, X.; Yang, J.; Zhu, L.; Wang, B.; Sun, G.; Lv, P.; Phang, I. Y.; Liu, T. J Appl Polym Sci 2006, 102, 542.
41. Gu, S.-Y.; Ren, J.; Wang, Q.-F. J Appl Polym Sci 2004, 91, 2427.
42. Ferry, J. D. Viscoelastic Properties of Polymers, 3rd ed.; Wiley: New York, 1980.
43. Shumsky, V. F.; Lipatov, Y.; Getmanchuk, I.; Usenko, A.; Cassagnau, P.; Boiteux, G.; Melis, F.; Lucas, J. M. J Appl Polym Sci 2006, 102, 2700.